Budapest University of Technology and Economics
Faculty of Electrical Engineering and Informatics
Department of Measurement and Information Systems

Force characteristic parameter identification of stepped pole solenoid actuator

Scientific Students' Association Report

Author:

Levente Palicsek

Advisor:

dr. Péter Stumpf
Dávid Baranyai

2023

Contents

Chapter 1

Introduction

Solenoid actuators (figure 1.1) are widely used in the automotive industry because of their simple, rugged construction and being relatively cheap to manufacture. They are often used as on/off or proportional valves. The characteristics of the magnetic force output of these actuators is greatly dependent on the construction of the solenoid, the air gaps, the movable core, and the pole piece.

Figure 1.1: Industrial solenoid valves [6]

In this paper, multiple mathematical models are constructed to determine the relationship between the air gap and driving current input, and the magnetic force output of a stepped pole solenoid. I compare multiple types of black box models and construct a grey-box model based on the physical properties of the system. Also, for the training of these models, the identified solenoid is driven by a driver chip that is widely used in the industry. This allows to build a more realistic model. Finally, I validated the models with independent measurements. The proposed method introduced in the paper can be used for other hardware components (driver circuits or solenoids) as well. As a contribution the developed models allow the design of controllers with higher performance and reliability, for solenoid valves.

In Chapter 2, I go over the basics of a solenoid actuator magnetic circuit and electrical model, and introduce the most common topologies and techniques used to control the current of such an actuator.

In Chapter 3, I describe the test environment, the measurement software, its functions and capabilities, and the measurement methods.

In Chapter 4, I describe the measurements conducted to capture the behavior of the stepped pole solenoid actuator.

In Chapter 5, I create different kinds of models based on the measurements.

In Chapter 6, I compare the models, and draw conclusions on which model works best by a number of criteria.

Chapter 2

Solenoids and current control

2.1 Solenoid model

2.1.1 Solenoid electrical model

A solenoid actuator (figure 2.1) is a device that uses electromagnetism to convert electrical energy into mechanical energy. From the electrical point of view, the solenoid valve represents essentially an inductive load due to the presence of the solenoid coil made of conductive material, with a ferromagnetic core.

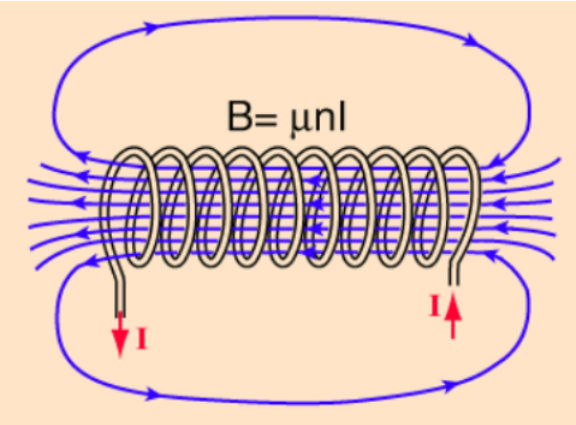

Figure 2.1: Magnetic field generated by a solenoid [1]

Supplying a current intensity I, a megnetic field $\vec{H}$ and its induction vector $\vec{B}$ will be generated in both the internal section and the outside area surrounding the coil, as shown in figure 2.1.

The inductance L is defined as the ratio between the magnetic flux ϕ and the electrical current I. It measures the solenoid capability of generating magnetic field when supplied with an electrical current.

$$L = \frac{\phi}{I} = \mu \frac{N^2 S}{l} \tag{2.1}$$

where μ is the magnetic permeability depending on the core material, N is the coil number, S is the area of the inner section, and l is the solenoid length.

The ideal electrical model would be only an inductive load, but there are multiple losses the ideal model does not account for. These losses need to be taken into account in order to create an accurate electrical model. There are mainly four losses:

- Losses due to Joule effect: this is due to the resistance of the coil material, losing power through heat as current passes through it. This effect can be modeled as a series resistor R_1, and the lost power is equal to $P = RI^2$.
- Losses due to dinghy imperfection: some field lines don't converge on the device axis, and limit the capability of transferring mechanical energy to the mobile core. This can be modeled with a series inductance X_1.
- Losses due to magnetization currents: the ferromagnetic core has a magnetization current lost from the supply current, which can be modeled by a parallel resistor R_0.
- Losses due to parasitic currents: since the core is moving, the magnetic flow through the material changes. Faraday's law of induction states that a variation of the magnetic flow ϕ through a section of a material generates and induced electromotive force. This phenomenon is responsible of parasitic currents inside the ferromagnetic core, known as Foucault currents, which contribute to overall losses. [1]

Putting it all together, the real electrical model is seen on figure 2.2.

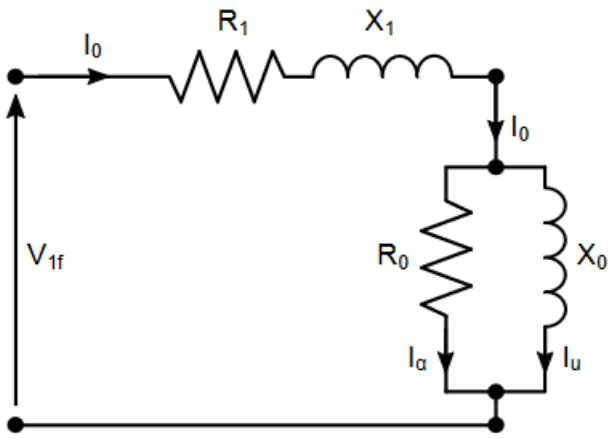

Figure 2.2: Real electrical model of a solenoid actuator [1]

2.1.2 Magnetic circuit

The simplified magnetic circuit can be seen on figure 2.3. The arrows indicate the path of the magnetic field lines. Air gaps represent magnetic resistance.

The force in air gaps according to Maxwell's law is:

$$F = \frac{(NI)^2 \mu S}{2x^2} \tag{2.2}$$

where I is the driving current, and x is the size of the air gap.

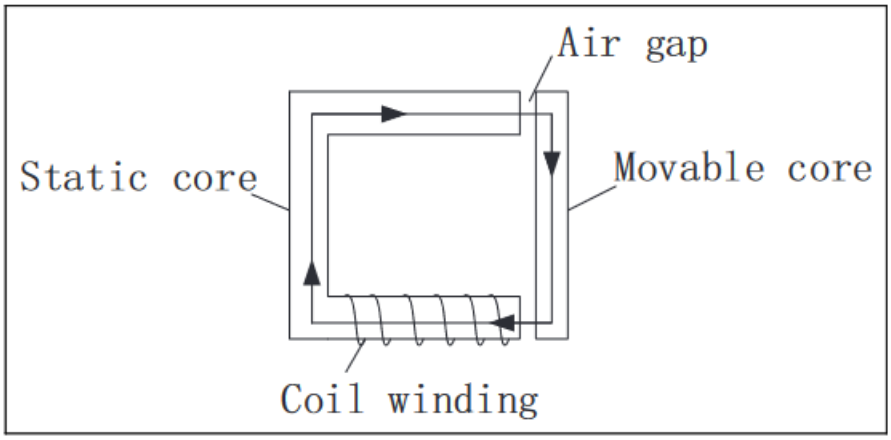

Figure 2.3: Magnetic circuit of a solenoid valve [16]

This model, however, does not take the construction of the static core (pole) and the movable core into account. There are many different designs, which produce different force characteristics, as described in [9].

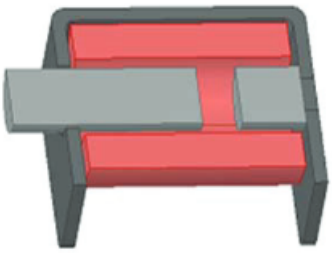

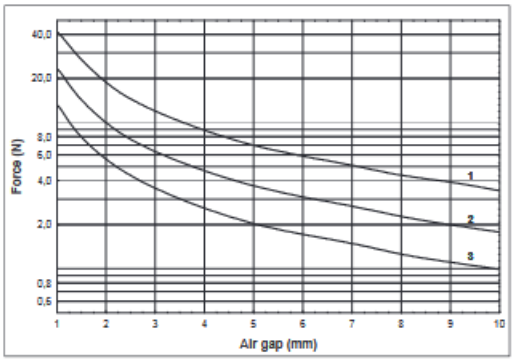

Figure 2.4: Construction and force characteristics of flat cylindrical pole solenoid [9]

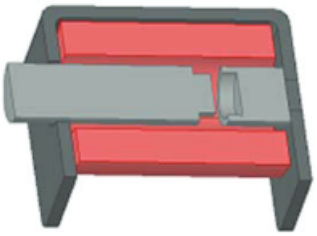

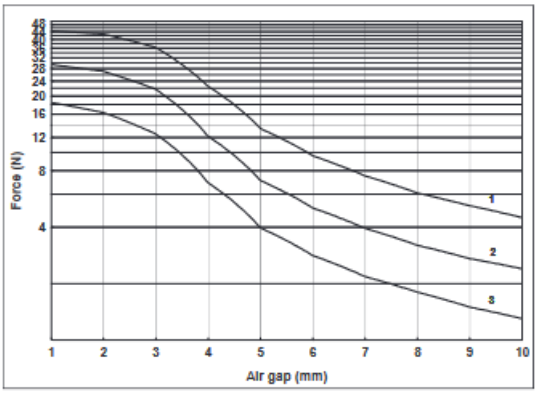

Figure 2.5: Construction and force characteristics of stepped cylindrical pole solenoid [9]

The force characteristics of the different pole designs are more complex, and can be modelled by finite element methods as in [9], but that is more costly and time consuming.

In this paper I aim to provide a simpler model to the stepped cylindrical solenoid's force characteristic.

2.2 Current control

Solenoid valves can be actuated by controlling the current of the coil. There are multiple methods of achieving this, depending on the application.

Driving solenoids with current control requires two things: the sensing and regulating of current. As the solenoid heats up from I^2R losses or is warmed by its environment, the coil resistance increases. With the current-sense feedback, the current can be monitored and adjusted to produce constant force even with the changes in resistance.

There are two methods for providing load current feedback from motor driver IC to a microcontroller. One method is from a current shunt amplifier using an external sense resistor that is either connected in line with the load, or on high- or low-side. The other is from a current mirror, which provides a proportional current to load current to pin output, removing the need for an external sense resistor.

To regulate current and energize and de-energize most solenoids, peak-and-hold drive is desired. The charging current is driven into the solenoid, called the peak current. The current in the solenoid will ramp ti its peak, at which point the magnetic field will depress the plunger into the spring (or pull it). To maintain the solenoid in position, current must still be driven into it, but this current is far lower than the peak current. This is referred to as hold current (figure 2.6). [5]

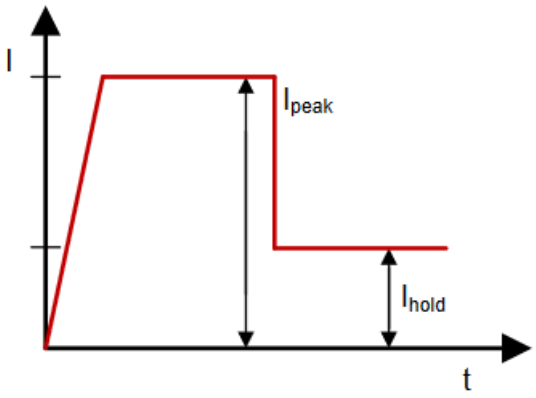

Figure 2.6: Peak and hold waveform [5]

2.2.1 Driver topologies

Most systems today use drivers to actuate and de-actuate solenoids. There are four basic configurations: low-side, high-side, half-bridge, and full-bridge (H-bridge).

High side driver protects against short to ground fault, whereas a low-side driver protects against short to battery fault. They use a single MOSFET (metal-oxide-semiconductor field-effect transistor) with enough current handling capacity to drive the solenoid.

When the MOSFET is enabled, it conducts all the current needed to energize the solenoid. When the MOSFET is disabled, the current in the solenoid must freewheel through a diode,

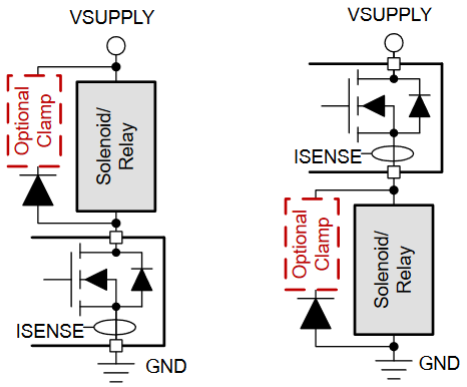

Figure 2.7: Low-side and high-side driver configurations [5]

or be allowed to continue flowing or decay to zero, otherwise the MOSFET can see large voltage spikes. This is apparent from the expression that defines the voltage characteristic of the inductors: $V = L \cdot di/dt$. The freewheeling diode across the solenoid provides this low impedance path for solenoid current to flow. [5]

A half-bridge driver uses two MOSFETs to control the current through a solenoid; one MOSFET to forward drive the solenoid, the other to recirculate the current.

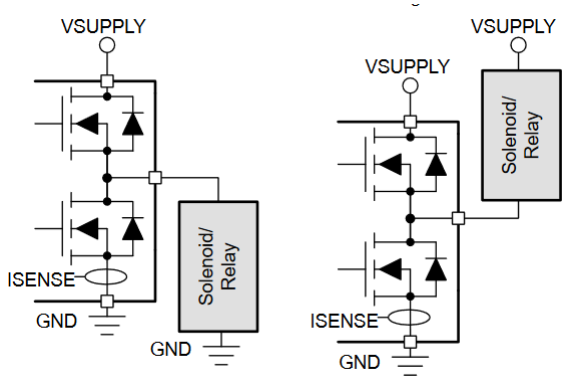

Figure 2.8: Half-bridge driver configurations [5]

The H-bridge driver uses four MOSFETs, or two half-bridges joined by a load, to control current through a solenoid. With four MOSFETs, bidirectional current control is possible.

The H-bridge driver can enable both slow and fast decay (coast) by recirculating current with either high- or low-side MOSFETs. Fast decay can be accomplished by turning off the MOSFETs and allowing current to flow through the body diodes. This results in an opposing voltage to the solenoid current equal to VM plus the forward voltage of the two body diodes. [5]

2.2.2 Current control methods

The current driving the solenoid can be controlled by periodically switching on and off MOSFET(s) of the driver. This is usually done by applying a pulse-width modulated (PWM) signal to them. The duty cycle of the PWM signal will set the amount of time current will flow through the solenoid, and the amount of time current will recirculate, thus setting the desired average current.

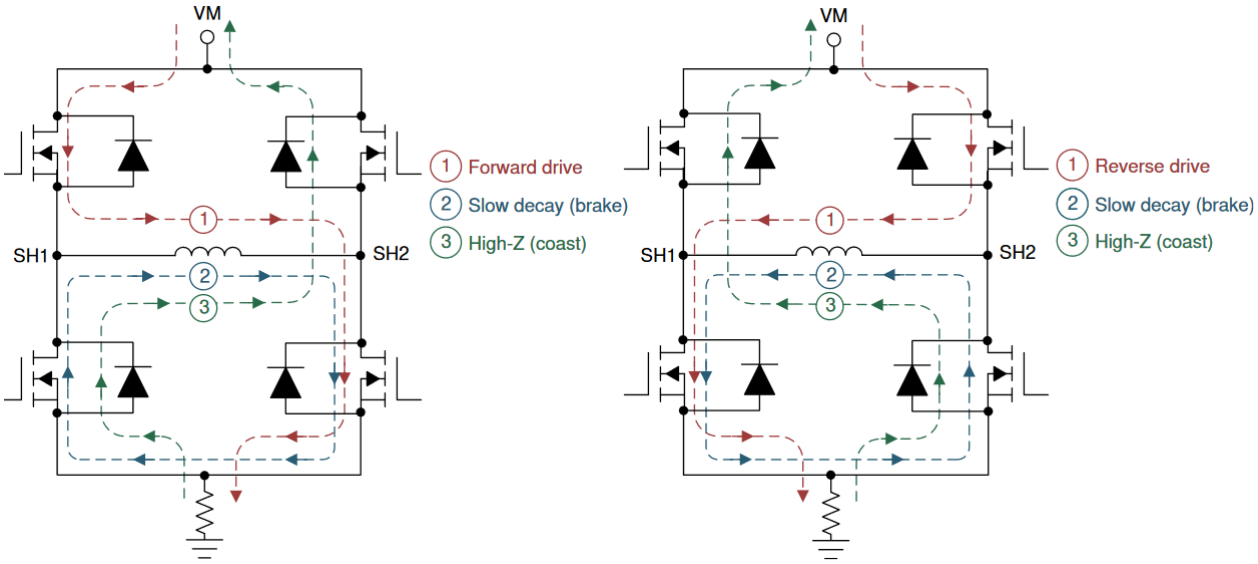

Figure 2.9: H-bridge driver configuration with current paths [5]

The resistance of the solenoid coil changes, as it heats up after prolonged operation, so some kind of current feedback is necessary. Most drivers provide current sense feedback at the FETs, to measure the error of the set current. Based on this error, some kind of controller algorithm calculates the necessary PWM duty cycle.

The most common traditional algorithm for this is the proportional-integral (PI) controller. The overall control function of the PI controller is the following:

$$u(t) = K_P e(t) + K_I \int_0^t e(\tau) d\tau \tag{2.3}$$

where $u(t)$ is the control signal at a time, $e(t)$ is the error signal, and K_P and K_I are coefficients for proportional and integral terms respectively.

There are multiple methods to increase the efficiency and robustness of the control algorithm. Some drivers allow for the use of variable frequency [2].

Another approach to improve control accuracy is the use of a dither signal. Because the core of the solenoid is usually made of ferromagnetic material, its magnetic field strength - magnetic induction curve has hysteresis, which can influence the accuracy of force control. Applying a sinusoidal dither current to the solenoid driver current can greatly reduce the hysteresis effect of the valve. [15] Also, keeping the mobile core constantly in motion, the effect of sticking friction becomes negligible.

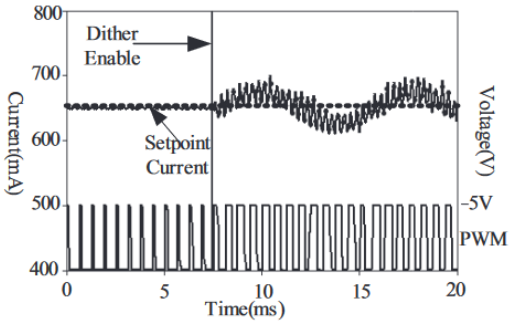

Figure 2.10: Dither waveform [15]

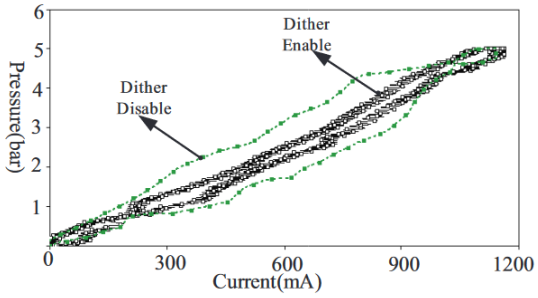

Figure 2.11: Hysteresis reduction effect of dither [15]

Chapter 3

Test environment

3.1 Test hardware

The test environment consists of two main parts: the current controller and the testbench.

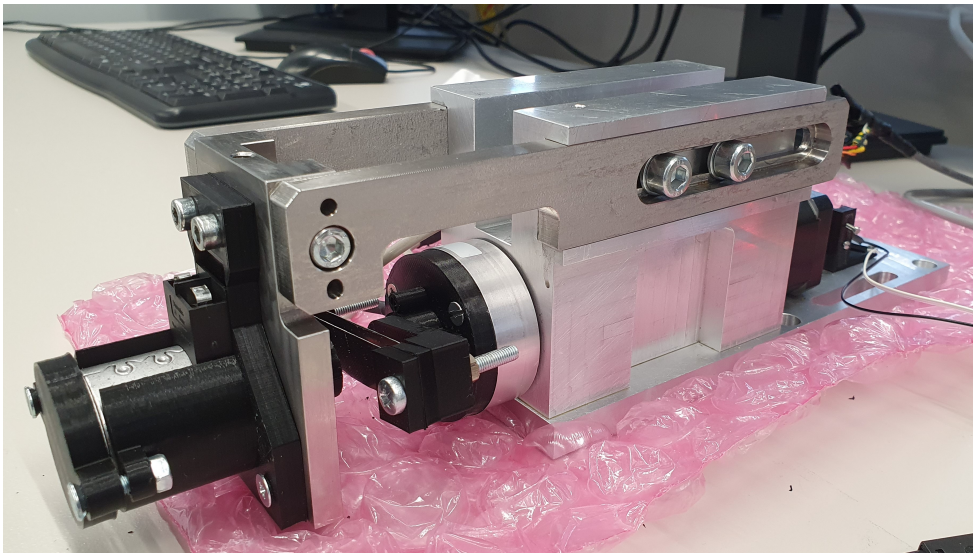

Figure 3.1: The testbench

The testbench consists of a stepper motor, a force sensor, and printed circuit board (PCB), which contains a microcontroller, a motor driver, USB connector and a CAN connector. The stepper motor is a linear actuator, which applies load onto the plunger of the analyzed solenoid through a spring system, or a static piece.

Between the axis of the linear actuator and the spring system/static piece, a force-cell Wheatstone-bridge sensor is placed, which outputs a differential signal based on the force applied to the solenoid. An amplifier circuit is added to the PCB, the output of which is read by the analog/digital converter (ADC) of the microcontroller.

The stepper motor can provide as much thrust as 300N on 24V, and can be moved with a step length of 0.01mm, which allows for a very precise setting of the air gap/load force.

The testbench is supplied from a laboratory DC power supply, at 24V. This is the voltage required by the stepper motor. This voltage is reduced by a to 3.3V in two steps, one Buck-converter from 24V to 5V, and one low-dropout regulator (LDO) from 5V to 3.3V.

The 3.3V supplies the microcontroller. The 5V excitation of the force sensor is created by an independent LDO from 24V to 5V. This voltage is monitored by the microcontroller and the amplified sensor signal is compensated by the change in excitation.

3.2 Test software

The control software of the testbench is seen on figure 3.2.

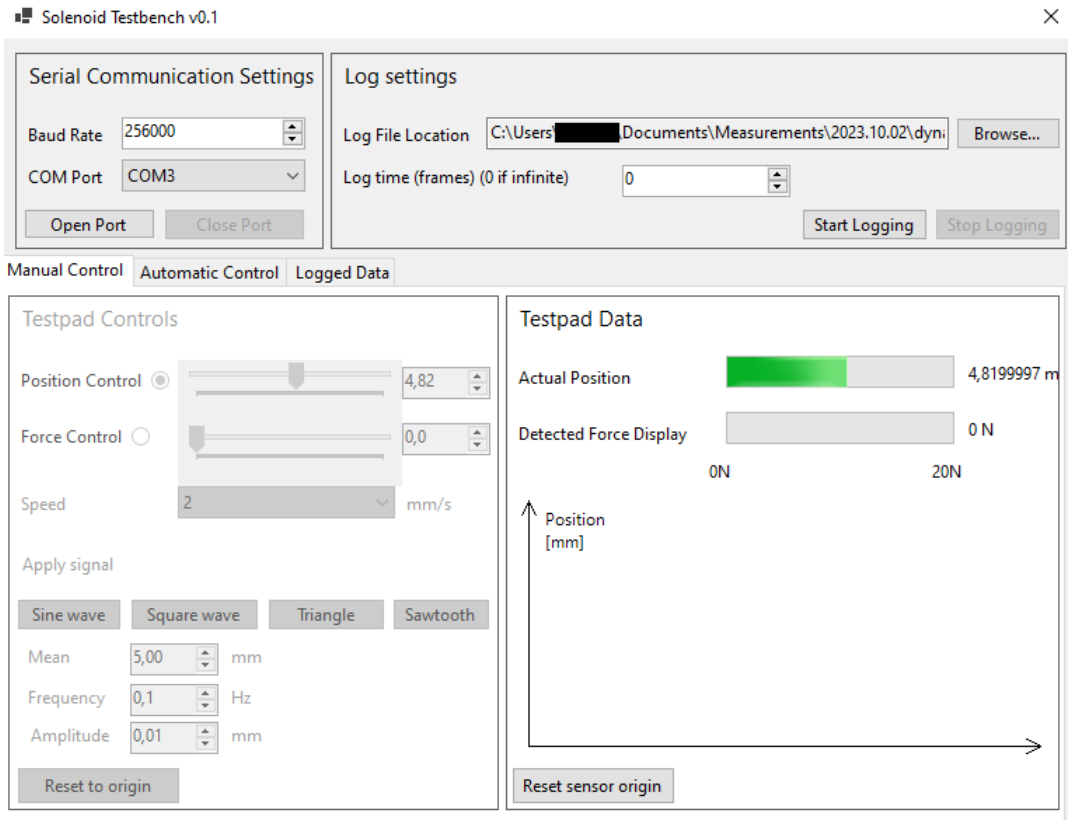

Figure 3.2: Testbench control software

This software allows for the position and force control of the testbench. Through force control, I can apply a desired amount of force to the plunger of the solenoid, and through position control I can manipulate the length of the air gap. In both force and position control modes, the software allows the application of a signal, such as sinus or triangle wave to the output.

The results can be logged into .csv files, and read back by the software for quick analysis (figure 3.3). On this figure the force control of the testbench software can be seen, which is achieved with a PI controller. As visible there is little overshoot and no static error, the rise time is limited by the maximum speed of the actuator.

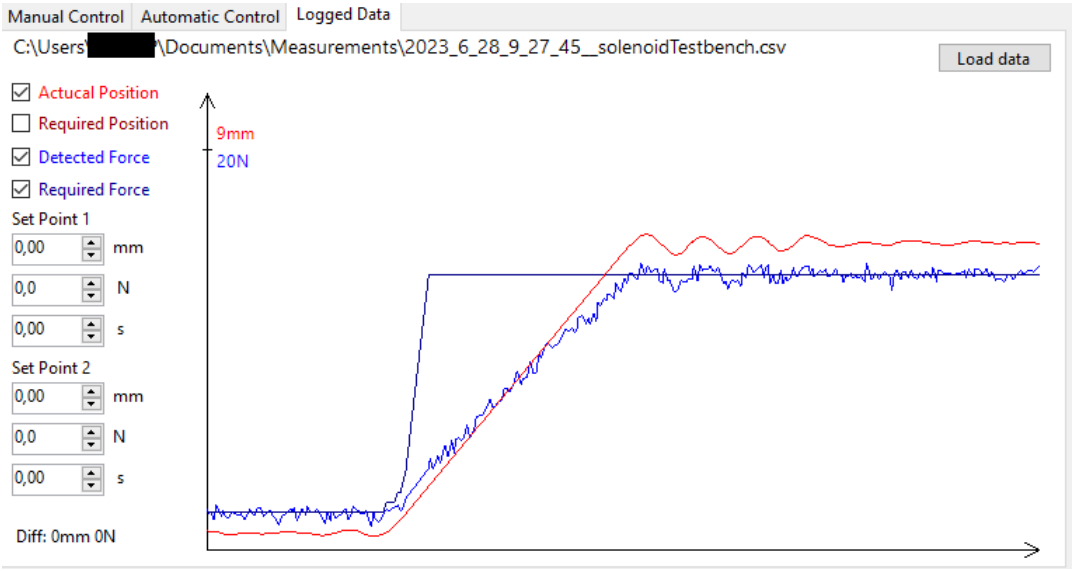

Figure 3.3: Measurement results quick view

There is an option to use predefined testing scripts for the measurements, which makes conducting complicated tests much easier and faster.

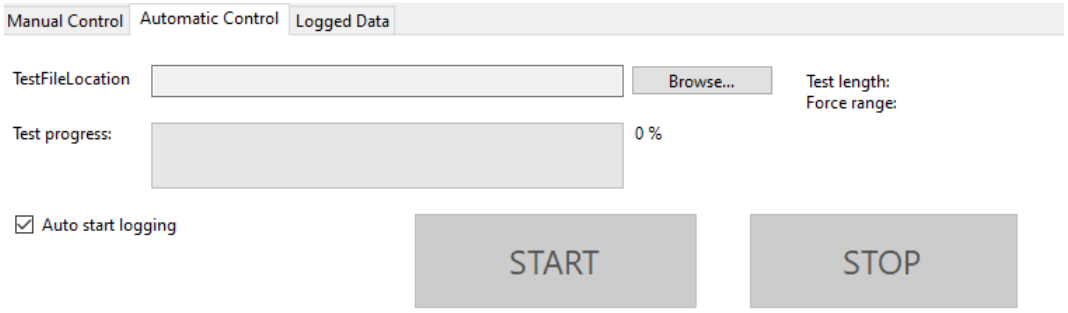

Figure 3.4: Automated test interface

3.3 Current control chip

To control the current of the solenoid actuator, I used a transmission control unit (TCU), which is already in mass production. The TCU includes an L9300 current control IC (U-chip), which provides 6 current control channels specifically designed to drive solenoid valves. Each channel includes the driving transistor, the recirculation transistor and the current sensing structure and can work in low-side driving mode with high-side recirculation or in high-side driving mode with low-side recirculation (figure 3.5).

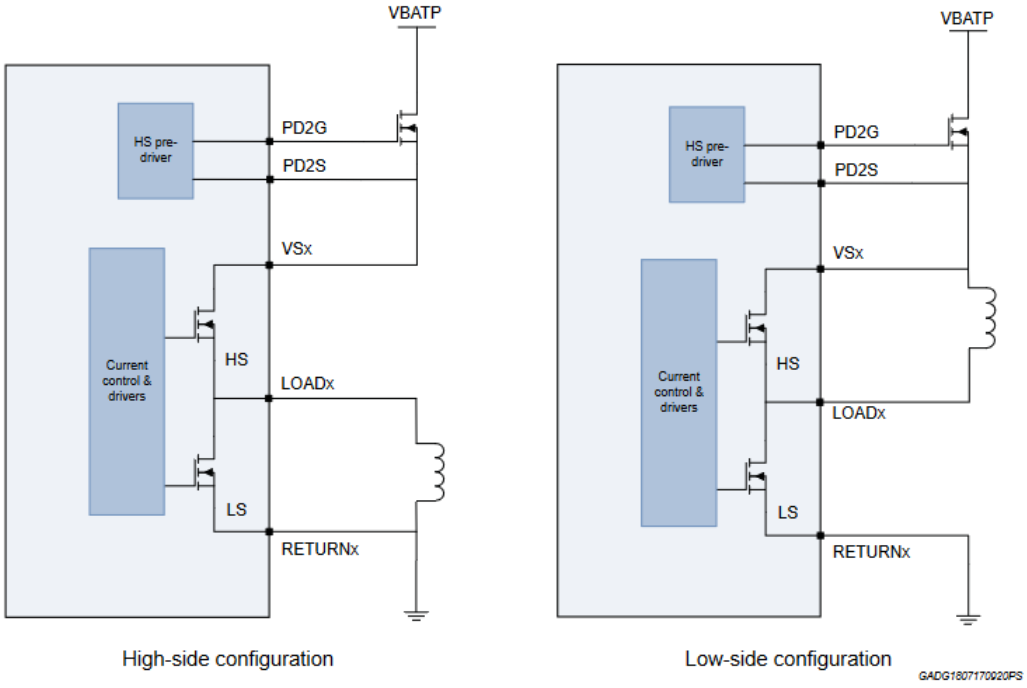

Figure 3.5: L9300 driver configurations [2]

The L9300 offers fixed and variable frequency current control algorithms, and programmable dither function. In this case, I only used fixed frequency with no dither applied.

Chapter 4

Measurements

For the identification of the force characteristics, the behavior of the solenoid needs to be measured under different circumstances. I categorized these measurements in two groups.

The first group of measurements are static measurements, that the plunger of the solenoid actuator remains fixed, so the length of the air gap does not change. These measurements allow the construction of a simpler model.

The second group of measurements are the dynamic measurements, in which the plunger is moving, while a driving current is applied to the coil.

4.1 Static measurements

To get the simplest idea of how the solenoid behaves, I measured the a series of current step responses at fixed stroke lengths.

Due to the switching nature of the driver IC, the current signal has ripples as it can be seen on figure 4.1. The magnitude of the ripples is inversely proportional to the switching frequency, and proportional to the magnitude of the inductance of the solenoid.

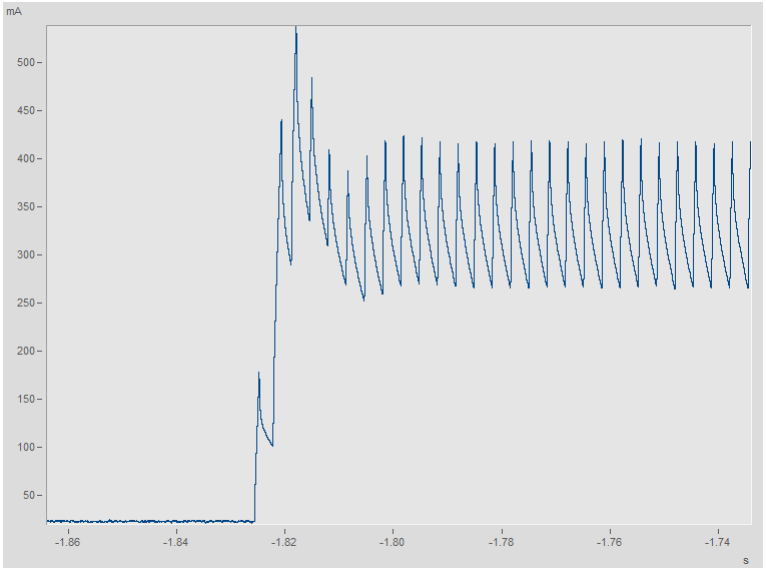

Figure 4.1: Current step waveform

The ripples in the current results in ripples in the force signal as well, as seen in figure 4.2.

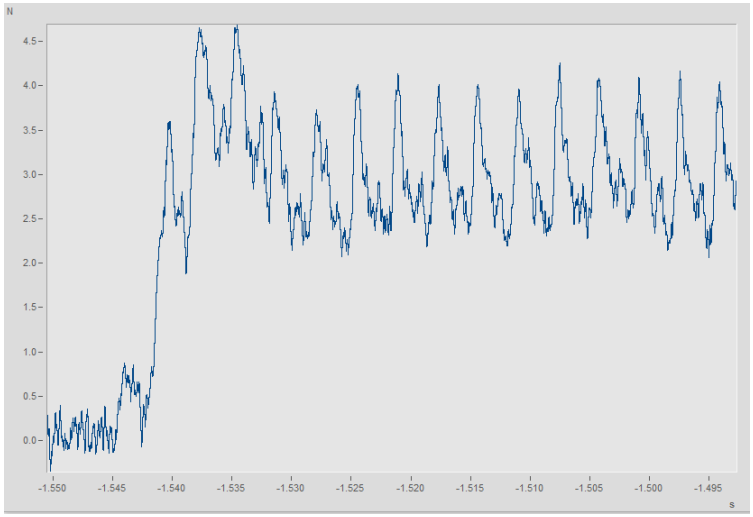

Figure 4.2: Force response to current step

For the fixed plunger position measurements, I applied a series of current steps from 300mA to 1200mA, with 80ms delays between rising and falling edges. I repeated these measurements for multiple plunger positions between the minimal and maximal air gap size.

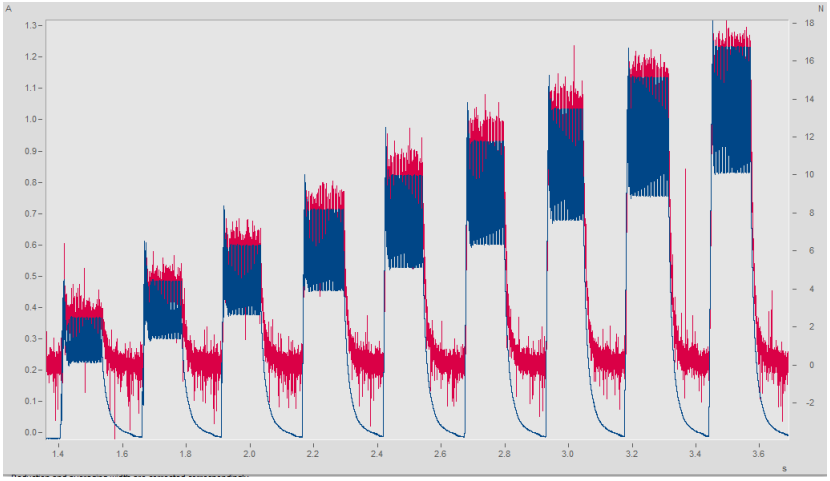

Figure 4.3: Magnetic force response of different current steps

From these experiments, I took the root mean square (RMS) value of the force steps, and plotted them against the current steps, so I could get multiple current-force curves (figure 4.4).

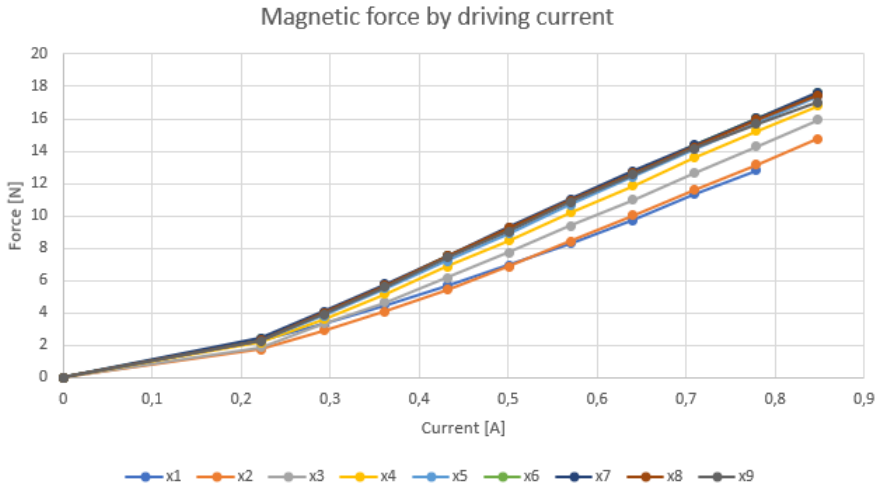

Figure 4.4: Magnetic force by driving current at different air gap lengths

From these same measurements, I plotted the RMS value of the force steps against the air gap size, since the current steps had been the same at all plunger positions (figure 4.5).

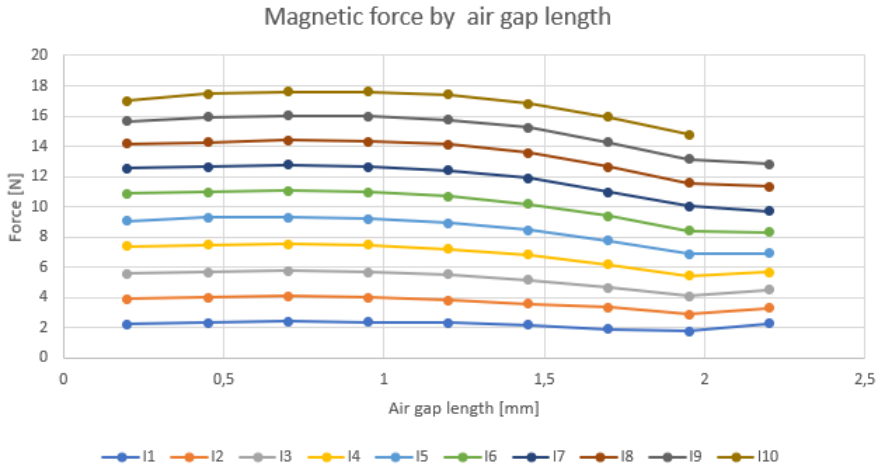

Figure 4.5: Magnetic force by air gap at different driving currents lengths

It is clearly visible, that the larger the driving current, the higher impact the air gap length has on the produced force. Also, the largest force is produced around the middle of the air gap range.

4.2 Dynamic measurements

Next, I measured the output force of the solenoid with static current, and gradually decreasing air gap. This way I get a continuous air gap-force characteristic, but the inertia of the moving core and viscous damping needs to be taken into account.

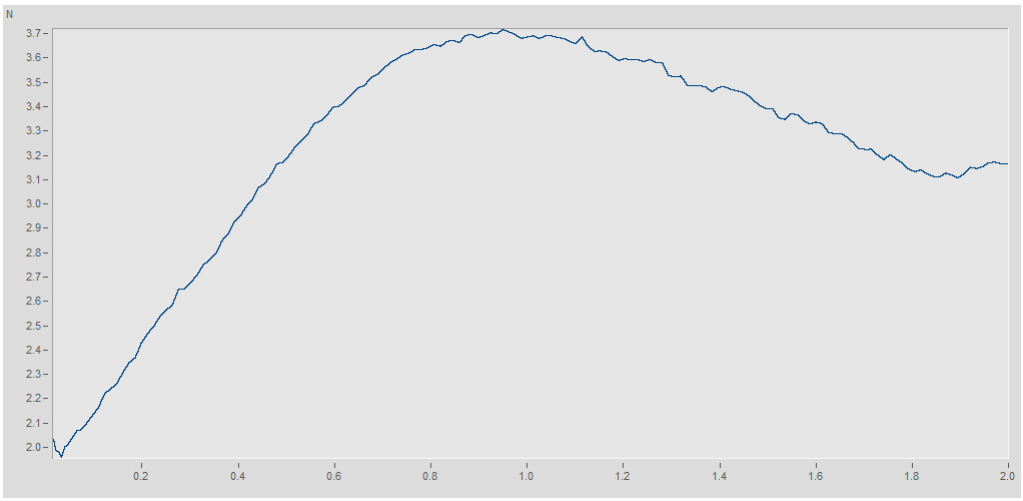

Figure 4.6: Magnetic force by plunger position at a specific current (filtered)

I repeated this measurement with increasing currents (figure 4.7). Because of the measurement setup, the dynamic measurements have much higher noise, which needed to be filtered more aggressively. This will decrease the accuracy of the dynamic simulations.

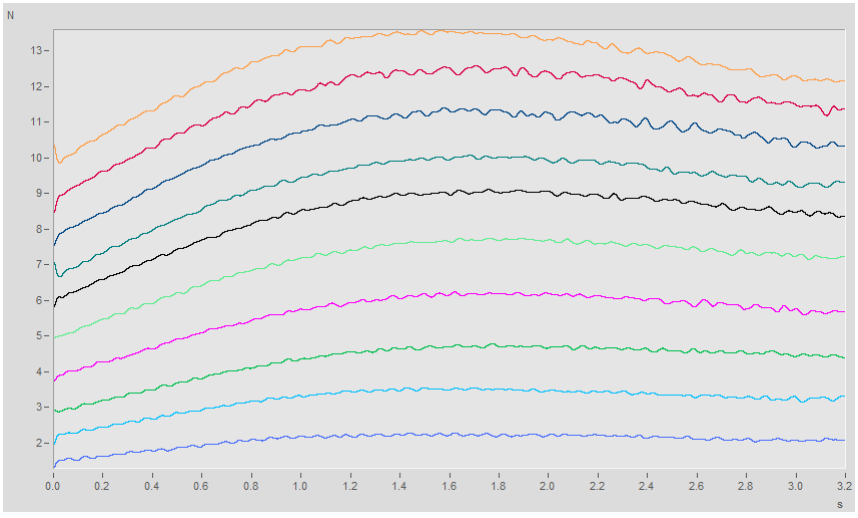

Figure 4.7: Dynamic measurements (filtered)

Chapter 5

Modeling

The desired model of the solenoid will take the air gap size (x) and driving current (i) as inputs, and produce the load force of the solenoid as output.

The mechanical differential equation of the system is as follows:

$$F_l + m\ddot{x} + \lambda\dot{x} = F_e \tag{5.1}$$

where F_l is the load force, m is the weight of the plunger, λ is the damping coefficient, and F_e is the electromechanical force. The objective of this paper is to find a simple model for F_e, which accurately describes the solenoid actuator.

According to Maxwell's law, the force in air gaps can be calculated in the form of Equation 2.2, but this equation does not take the construction of the magnetic circuit into account. However, it is clear that the force output is at least a second degree polynomial of the inputs.

To find a model, which can more accurately describe the behavior of the stepped pole solenoid, I fitted second degree polynomials on the RMS current step responses (figure 4.3), and plotted them against the air gap length.

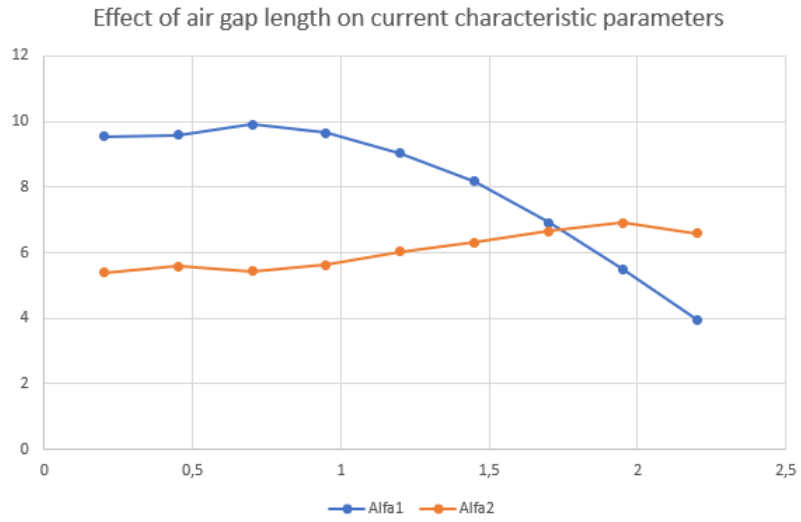

Figure 5.1: $F = \alpha_2 i^2 + \alpha_1 i$ parameters by air gap length

One thing, that is immediately visible from the measurements that the magnetic force has a slight delay to the driving current (figure 5.2), which is due to magnetic diffusion.

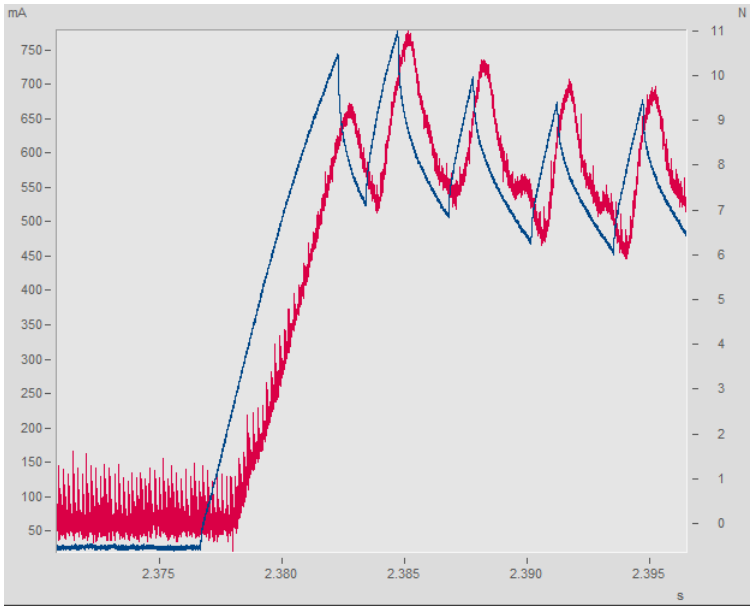

Figure 5.2: Delay of magnetic force (red) to driving current (blue)

I approached this problem with two main methods. In the first method, I tried multiple types of black-box systems and compared their accuracy. In the case of a black-box model, the exact structure of the model is unknown, and it is trained with the measured output response for known inputs.

The other approach is the grey-box method. In this case, I used my knowledge of the physical system to construct a model, in which only the constant parameters are unknown. Then, these parameters are identified through optimization methods based on the measurements.

I used MATLAB's System Identification Toolbox to construct and optimize these models. For training and model optimization, I used the only the measurements preformed on the first solenoid, and for validation, I used the measurement data from another solenoid of the same type.

The percentages on the validation plots are fit values calculated by equation 5.2.

$$fit = 100(1 - \frac{||y - \tilde{y}||}{||y - mean(y)||}) \tag{5.2}$$

where y is the validation data, and $\tilde{y}$ is the output of the compared model. This equation works well with fixed measurements, but doesn't define fitness very well for the dynamic measurements.

5.1 Black-box models

5.1.1 Linear black-box model

The force response of the solenoid is clearly nonlinear, but as a simplification I tried to fit a linear models to it before moving on to non-linear models.

The simplest black-box model is the transfer function. In this case only the number of poles and zeroes need to be set. The pole-zero representation of a transfer function with n poles and m zeros is as equation 5.3.

$$G(s) = \frac{\prod_j^n (s - z_j)}{\prod_i^m (s - p_i)} \tag{5.3}$$

The best fit for the data was a transfer function with two poles and no zeros.

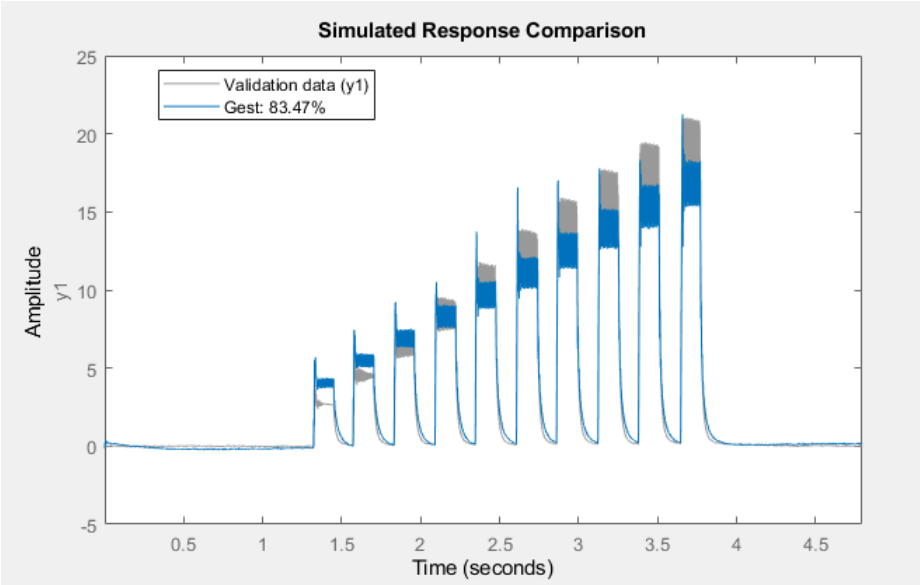

Figure 5.3: Estimated transfer function

As seen on figure 5.3, a linear transfer function can capture the waveform of the output, but it can not accurately predict the mean of the step responses, since they follow a nonlinear function.

5.1.2 Nonlinear black-box models

5.1.2.1 Nonlinear ARX model

The nonlinear ARX model (figure 5.4) is an extension of the linear ARX model, which is defined as equation 5.4.

$$A(q)y(t) = \sum_{i=1}^{nu} B_i(q)u_i(t - nk_i) + e(t) \tag{5.4}$$

where q is the time-shift operator, and $e(t)$ is a white-noise model. $A(q)$ and $B_i(q)$ contain the regressors, which in the linear case are past or present values of the inputs and output, and the linear combination of these is the present output. The coefficient of these regressors are the parameters to be optimized.

In the nonlinear case, I have the option to add nonlinear regressors, for example $u_1^2 \cdot u_2$. There is a delay built into nonlinear model, which helps describe the magnetic diffusion of the solenoid. There is an option to use nonlinear functions like wavelet, sigmoid, or even neural networks, but the nonlinear regressors with delay were adequate in this case.

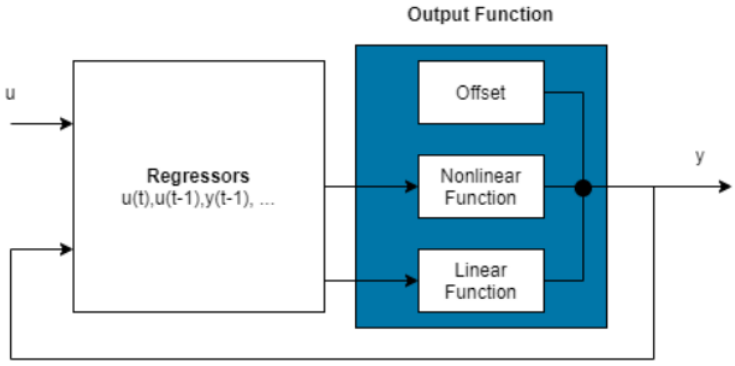

Figure 5.4: Structure of the nonlinear ARX model [3]

Based on figure 5.1, the parameters of u_1^2 can be expressed as a linear function of u_2, so this gives two regressors: $u_1^2 u_2$ and u_1^2. The parameters of u_1^2 can be expressed as a second-degree function of u_2, which gives three regressors: $u_1 u_2^2$, $u_1 u_2$ and u_1. I also added linear regressors to the output from (t-1) to (t-5), and from (t) to (t-5) for the inputs. All the nonlinear regressors go from (t) to (t-5). This helps better capture the dynamic behavior of the actuator.

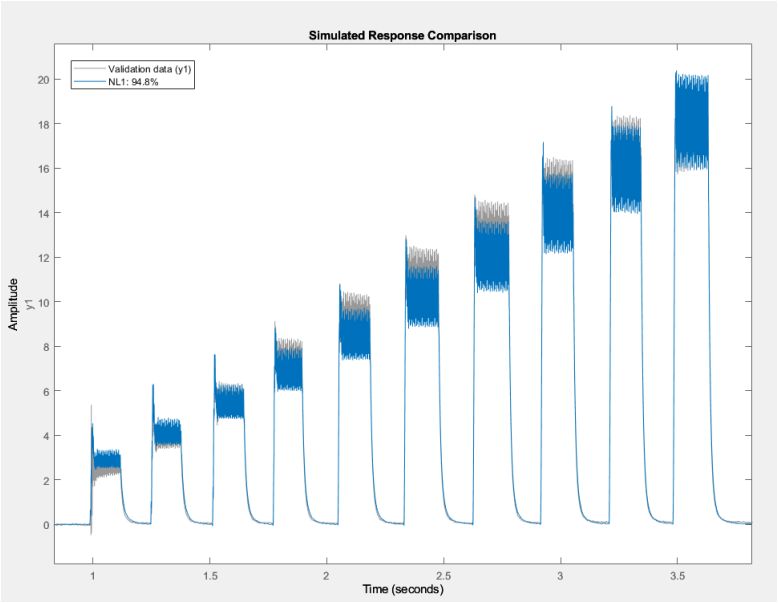

Figure 5.5: The non linear ARX model result compared to fixed data

As seen on figure 5.5 and figure 5.6, this model follows the solenoid behavior quite well, and the delay is mostly compensated, but it has 127 regressors, and requires a lot more computation than any of the other models described above.

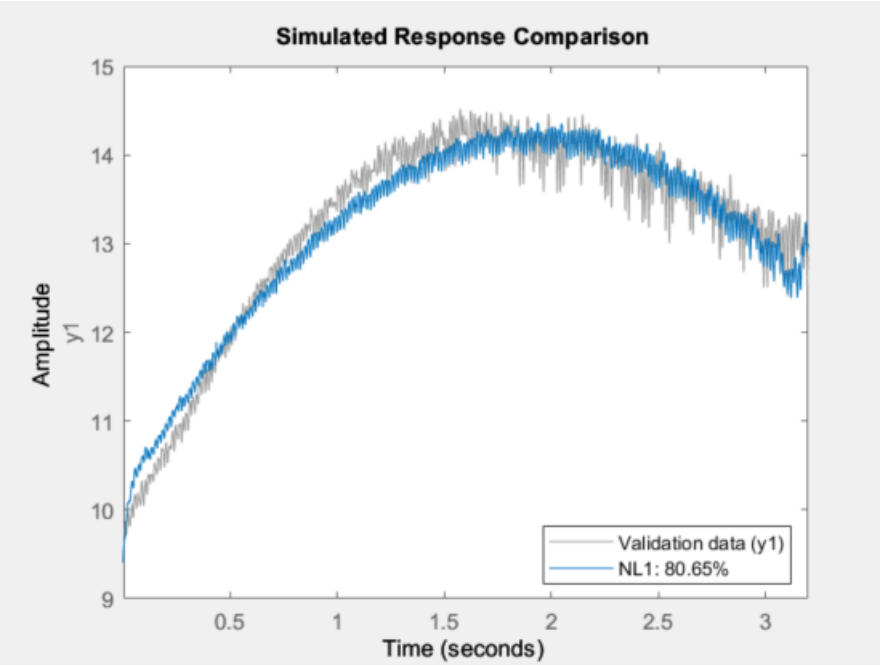

Figure 5.6: The non linear ARX model result compared to dynamic data

5.1.2.2 Neural state-space model

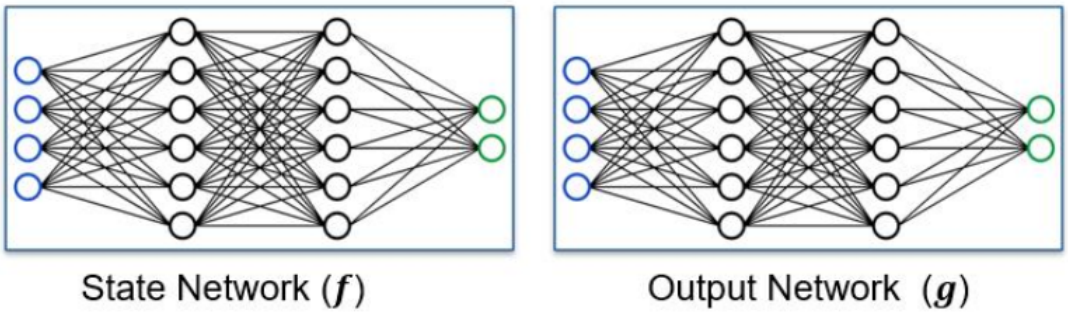

Figure 5.7: Neural state-space model [4]

Neural state-space models are a type of nonlinear state-space models where the state-transition and measurement functions are modeled using neural networks. A nonlinear state-space model has the following form:

$$\dot{x} = f(x, u, t, \theta_1) \tag{5.5}$$

$$y = g(x, u, t, \theta_2) \tag{5.6}$$

f and g are multi layered feed forward neural networks, trained on the measurement data. In this case, I used only one state, and chose it as the output $y = x$.

To set up the state network, the following parameters need to be set: number of hidden layers, number neurons per each layer, activation function for the hidden layers, weight and bias initialization. Since the model is not linearly separable, the number of hidden layers need to be higher than 0. I chose two hidden layers, and experimented with the neuron count. There are many rules of thumb when deciding the neuron count of the hidden layers, but generally it should be between the number of inputs and outputs. In this case, the state network has three inputs (u_1, u_2, and x) and one output dx. For faster learning, I chose than tanh activation function, for which the 'glorot' weight initializer is recommended. For the bias initializer I chose 'zeros'.

The training data needed some extra pre-processing in this case. First, I normalized all inputs and outputs between one and zero, then split up the experiments into multiple overlapping pieces, each about 30 milliseconds long. This way, the neural network was able to learn much faster than with larger data chunks.

First I trained the model with 2 hidden layers with 2 neurons each, with 'adam' optimizer. The results can be seen on figure 5.8.

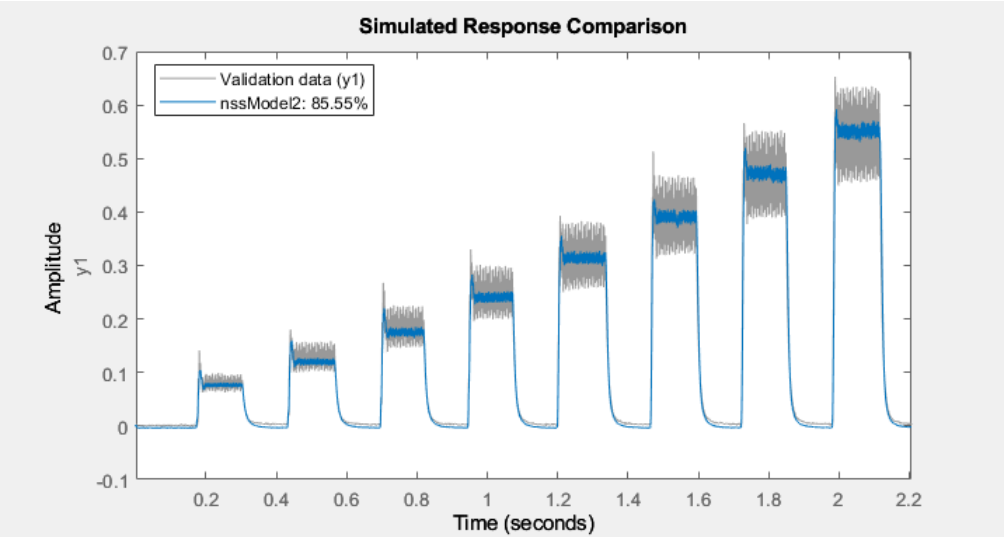

Figure 5.8: 2 hidden layers 2 neurons state network results

I also trained a model with 2 hidden layers with 3 neurons each, with the same settings as above to see if it could preform better at higher complexities (figure 5.9). It made some difference, but it raised the simulation time by about 50%.

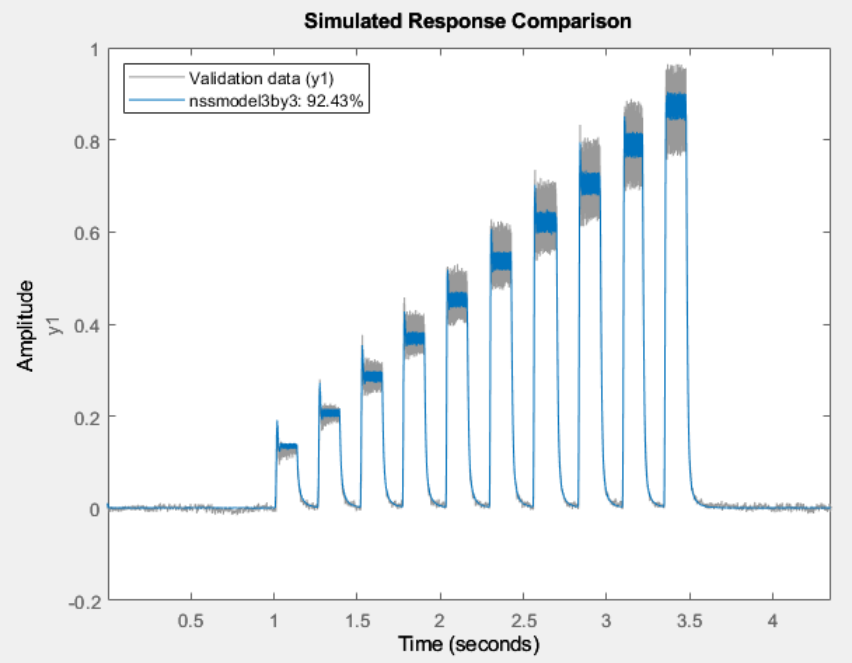

Figure 5.9: 3 hidden layers 3 neurons state network results

With this model, the delay due to magnetic diffusion is eliminated completely, and the mean values of the step responses are also very close to the real response. However, the amplitude of the oscillating force is far from the real value, and this model took a long time (15 hours) and 10000 epochs to train, which could be problematic if it has to be retrained for different solenoids.

5.2 Grey-box model

When constructing my grey-box model, I started out from the non-moving measurements.

The non-linear grey box model I chose uses the following form: The output of the model and the derivative of the states must be given as a function of the inputs, the states and the parameters to be optimized.

$$y = F(t, x(t), u(t), par1, par2, ..., parN) \tag{5.7}$$

$$y(t) = H(t, x(t), u(t), par1, par2, ..., parN) + e(t) \tag{5.8}$$

$$x(0) = x_0 \tag{5.9}$$

As seen on figure 5.1, the α_0 parameter is nearly 0, which seems valid because at zero current there is no magnetic field. The α_2 parameter can be represented by a linear equation, and α_1 by a second degree polynomial. This way, the first grey box model, for a non moving solenoid is:

$$y = (\beta_{21}u_2 + \beta_{20})u_1^2 + (\beta_{12}u_2^2 + \beta_{11}u_2 + \beta_{10})u_1 \tag{5.10}$$

where the output is the magnetic force ($y = F_e$), the two inputs are the driving current ($u_1 = i$), and the air gap ($u_2 = x$).

For fixed position measurements, this model works quite well, there are larger errors on smaller current steps, but considering the simplicity of the model the results are adequate.

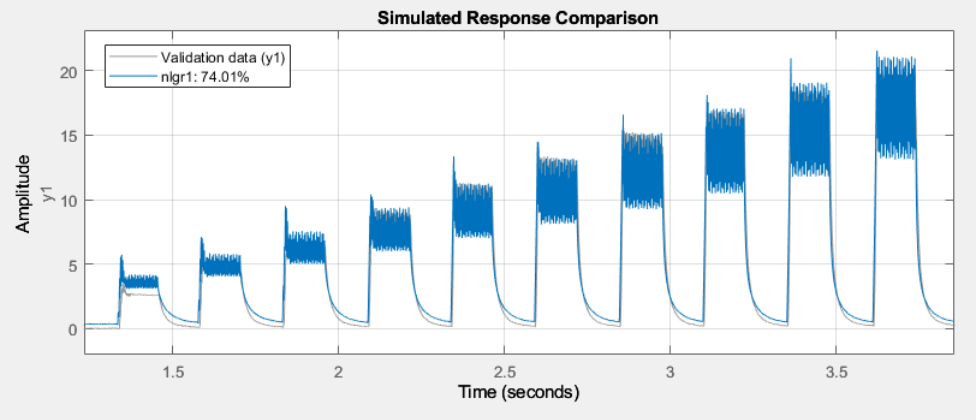

Figure 5.10: Fixed position grey-box model

The main problem with this model is that it doesn't account for the delay between the current input and the force output, which is due to magnetic diffusion. To account for it, I added a state to the model, which is equal to the output. The derivative of this state is the difference between the output of the previous model and the current output, multiplied by a diffusion parameter d.

$$\frac{dx}{dt} = (x - ((\beta_{21}u_2 + \beta_{20})u_1^2 + (\beta_{12}u_2^2 + \beta_{11}u_2 + \beta_{10})u_1)) \cdot d \tag{5.11}$$

For the parameter optimization of this model I used the β parameters from the previous fixed position model, and only optimized for the diffusion parameter d. As seen on figure 5.11, the delay is now compensated.

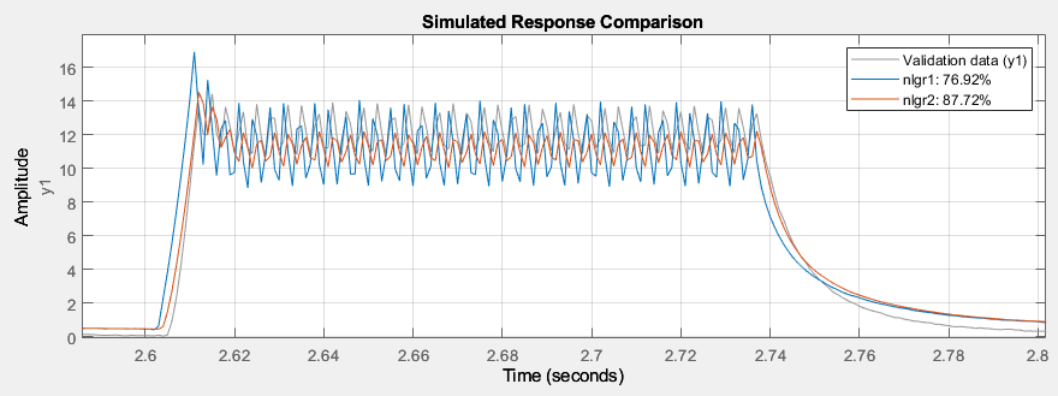

Figure 5.11: nlgr1: Original fixed position model, nlgr2: Model with diffusion delay

Next, I re-optimized these same two models to the fixed data merged with the dynamic measurements, to see how well the grey-box model preforms with the moving plunger.

As seen on figure 5.12, the model fits the curve quite well. It could be optimized with higher-degree polynomials of the air gap, but that would increase the computation cost.

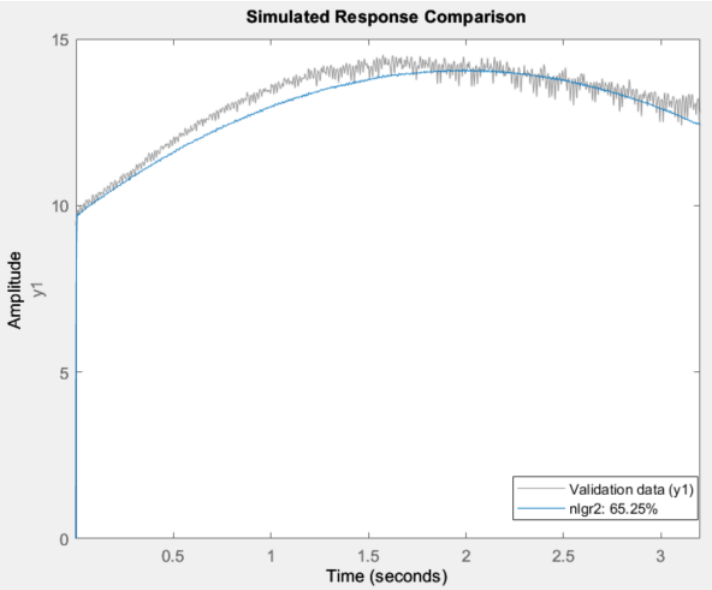

Figure 5.12: Greybox model compared to a dynamic measurement

I experimented with adding the viscous damping and inertia of the moving core to the model, but it made no significant difference at the velocities in the dynamic measurements, while driving up the complexity, so I left them out.

Chapter 6

Conclusions

In conclusion, the models proposed all capture the basic behavior of the stepped pole solenoid, some better in some aspects than the others. I compared the models by a number of criteria. Accuracy of fixed behavior, accuracy of dynamic behavior, accuracy at lower currents, complexity (or how much computation power does it require), and ease of training.

Model	Fixed accuracy	Dynamic accuracy	Low current accuracy	Complexity	Ease of training
Non-linear ARX	90-95%	High	High	High	Easy
Neural state-space	85-95%	Low	Medium	Medium	Difficult
Grey-box	80-90%	Medium	Low	Low	Medium

In terms of accuracy, the non-linear ARX model proved to be the best, especially in the case of the dynamic simulation. However, this is the most complex model, and this takes the most computational power to simulate. The setting up of the optimization and preparing data was the easiest task with this model.

The second in accuracy was the neural state space model. It provides low accuracy dynamic simulation, but excellent static simulation with good low current accuracy, and its computational draw is much better than that of the ARX. However, if this model ever needs to be retrained, it takes a significant time, and the preprocessing of the data is also more time consuming.

The simplest model is the grey-box, which for its complexity still provides good static accuracy, which decreases around the lower currents. It also preformed fairly well in dynamic simulations, though at lower currents the accuracy is quite low.

To further develop these models, I would increase their dynamic accuracy by using more estimation data with different movement speeds or multidirectional movement. Also, the measurement equipment's vulnerability to noise is far from ideal, and could be improved. The effect of the air gap length could also be estimated by a higher degree polynomial in the grey box model, or with more regressors in the ARX case.

Bibliography

[1] ST Microelectronics: Electrovalves: Principle of operation. https://www.st.com/resource/en/application_note/an5665-electrovalves-principle-of-operation-stmicroelectronics.pdf. Accessed: 2023-08-16.

[2] ST Microelectronics: Automotive flexible u-chip for braking and transmission. https://www.st.com/resource/en/datasheet/l9300.pdf. Accessed: 2023-08-19.

[3] MATLAB: What are nonlinear arx models? https://uk.mathworks.com/help/ident/ug/what-are-nonlinear-arx-models.html. Accessed: 2023-10-09.

[4] MATLAB: Neural state-space model of simple pendulum system. https://uk.mathworks.com/help/ident/ug/training-a-neural-state-space-model-for-a-simple-pendulum-system.html. Accessed: 2023-11-02.

[5] Texas Instruments: Using motor drivers to drive solenoids. https://www.ti.com/lit/an/slvae59a/slvae59a.pdf?ts=1688988811784&ref_url=https%253A%252F%252Finternet-start.net%252F. Accessed: 2023-08-18.

[6] Industrial solenoid valves. https://www.danfoss.com/en-us/products/sen/valves/solenoid-valves/industrial-solenoid-valves/. Accessed: 2023-10-23.

[7] M. Fauri and P. Sonato. A finite element analysis of an electromagnetic flow control valve. *IEEE Transactions on Magnetics*, 27(5):3912–3915, 1991. DOI: 10.1109/20.104958.

[8] Michele Folgheraiter. A combined b-spline-neural-network and arx model for online identification of nonlinear dynamic actuation systems. *Neurocomputing*, 175:433–442, 2016. ISSN 0925-2312. DOI: https://doi.org/10.1016/j.neucom.2015.10.077. URL https://www.sciencedirect.com/science/article/pii/S0925231215015362.

[9] Dian Malamov, Ivan Hadzhiev, and Ivan Yatchev. Influence of the pole shapes on the force characteristics of a dc solenoid actuator. In *2017 15th International Conference on Electrical Machines, Drives and Power Systems (ELMA)*, pages 435–438, 2017. DOI: 10.1109/ELMA.2017.7955480.

[10] D. Saravanakumar, B. Mohan, and T. Muthuramalingam. A review on recent research trends in servo pneumatic positioning systems. *Precision Engineering*, 49:481–492, 2017. ISSN 0141-6359. DOI: https://doi.org/10.1016/j.precisioneng.2017.01.014. URL https://www.sciencedirect.com/science/article/pii/S0141635916302574.

[11] Xue-ling Song, Ying-bao Zhao, Chao-ying Liu, and Zhe-ying Song. Solenoid valve switching characteristic test system design. In *2009 Ninth International Conference on Hybrid Intelligent Systems*, volume 3, pages 388–391, 2009. DOI: 10.1109/HIS.2009.291.

[12] M. Taghizadeh, A. Ghaffari, and F. Najafi. Modeling and identification of a solenoid valve for pwm control applications. *Comptes Rendus Mécanique*, 337(3):131–140, 2009. ISSN 1631-0721. DOI: https://doi.org/10.1016/j.crme.2009.03.009. URL https://www.sciencedirect.com/science/article/pii/S1631072109000308.

[13] Ngoc Anh Duy Hoang Minh Tri Nguyen Cong Toai Truong Huy Hung Nguyen Van Tu Duong, Quoc Minh Lam and Tan Tien Nguyen. Development of testing apparatus for investigating electromagnetic dynamics of contactors: A pilot study. *Instrumentation Science & Technology*, 0(0):1–17, 2023. DOI: 10.1080/10739149.2023.2259976. URL https://doi.org/10.1080/10739149.2023.2259976.

[14] Fangwei Xie, Rui Zhou, Dengshuai Wang, Jun Ke, Xinjian Guo, and Van Xo Nguyen. Simulation study on static and dynamic characteristics of electromagnet for electro-hydraulic proportional valve used in shock absorber. *IEEE Access*, 8:41870–41881, 2020. DOI: 10.1109/ACCESS.2020.2976713.

[15] Qirui Xu, Guo Wei, and Xingzhong Li. Characteristic analysis and control for high speed proportional solenoid valve. In *2013 IEEE 8th Conference on Industrial Electronics and Applications (ICIEA)*, pages 1578–1582, 2013. DOI: 10.1109/ICIEA.2013.6566620.

[16] Xiang Zhang, Yonghua Lu, Yang Li, Chi Zhang, and Rui Wang. Numerical calculation and experimental study on response characteristics of pneumatic solenoid valves. *Measurement and Control*, 52:002029401986685, 10 2019. DOI: 10.1177/0020294019866853.